

# An Experimental System for Time-Domain Microwave Breast Imaging

Emily Porter, Adam Santorelli, Mark Coates, and Milica Popović

*Department of Electrical and Computer Engineering, McGill University  
3480 University Street, Montreal, QC, Canada  
{emily.porter, adam.santorelli}@mail.mcgill.ca  
{milica.popovich, mark.coates}@mcgill.ca*

**Abstract** – This paper presents a time-domain system for microwave breast cancer detection. The experimental system uses wideband antennas and improved tissue phantoms. Results showing tumor detection using the proposed system are given for various tumor sizes and locations, as well as for different antenna arrangements. Favorable layouts of the antenna array are identified.

## I. INTRODUCTION

Microwave breast imaging is currently being researched as a method for detecting malignant tissue within the breast. It is based on the reported contrast in the dielectric properties of healthy tissue and tumors over the microwave frequency range [1]. Microwave imaging has the potential to be a complementary modality to standard detection techniques (x-ray mammography, ultrasound, magnetic resonance imaging) in that it would be non-invasive, painless, and would require no ionizing radiation [2], [3].

In this paper, we present an experimental system for monitoring breast health with time-domain microwave imaging. First, we briefly discuss breast phantoms which, mimicking the conductivity and relative permittivity of actual breast tissue, are used here to test the system. We also characterize an antenna that was previously designed for microwave breast imaging by offering simulation and measurement results. We then describe the experimental components and set-up in detail. Finally, we present preliminary experimental results achieved using phantoms with various sizes and locations of tumors, as well as with several antenna array layouts.

## II. METHODOLOGY

### A. Tissue Phantoms

The recipe for the breast phantoms, consisting of readily available chemicals, was adjusted through repeated experimentation so that the dielectric properties of the phantoms closely match those reported for actual breast tissue in [1], [4]–[6]. We constructed four types of phantoms, one each to approximate fat, gland, tumor and skin tissue in terms of their relative permittivity and conductivity at microwave frequencies. We presented the details of the phantom construction earlier in [7], describing the required chemical concentrations and the experimentally-observed dielectric properties.

### B. Antenna Characterization

The antenna used in this system is the Traveling Wave Tapered and Loaded Transmission Line Antenna (TWTLTLA), reported in [8]. It is a planar antenna, designed to be broadband using constant resistive loading. The antenna is formed using a tapered transmission line with a characteristic impedance of  $50\ \Omega$ . It has a resistively loaded section fabricated with a conductivity of  $1142.8\ \text{S/m}$  (a surface resistivity of  $50\ \Omega/\text{square}$ ). The antenna operates best in a medium of relative permittivity  $\epsilon_r = 10.2$ , which matches that of the antenna substrate, chosen strategically to have a value close to that of the average healthy breast tissue. The antenna has dimensions of  $0.635 \times 12 \times 15.8\ \text{mm}^3$ , appropriately compact for our application. It has signal fidelity above 0.95 and radiation efficiency of 39.21%. Figure 1 shows a photograph of the antenna.

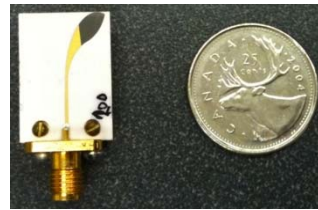


Fig. 1 The TWTLTLA, shown next to a Canadian quarter for scale.

In our system, the antennas are held in place by a radome (machined from our design by Friatec, [9]). It is a hemispherical shaped bowl inside of which sits the breast phantom. The antennas are inserted in 16 slots along the outer surface of the radome. The purpose of the radome is two-fold: to keep the phantom and antennas at precise locations for the repeatability of measurements, and, to provide a medium well-matched to the antenna to decrease the immediate return loss. The radome is made from Alumina, and has a relative permittivity  $\epsilon_r = 9.6$ . A photograph of the radome is shown in Figure 2, along with a drawing that shows all relevant dimensions.

The simulated and measured return loss,  $S_{11}$ , for the antenna in air and in the radome are shown in Figures 3 and 4, respectively. For this measurement, the radome is filled with the fat-mimicking material. All simulations were performed using the software tool SEMCAD X (SPEAG, [10]). We note

that the antenna has poor behaviour in air; however, it exhibits an improved  $S_{11}$  when it is placed inside the radome. From the plot, it is also evident that the measurement performed using the radome is noisier than that done in air. This is to be expected since, despite best efforts, slight air gaps between the antennas and the radome, and the radome and the phantom are inevitable and can cause signal distortion.

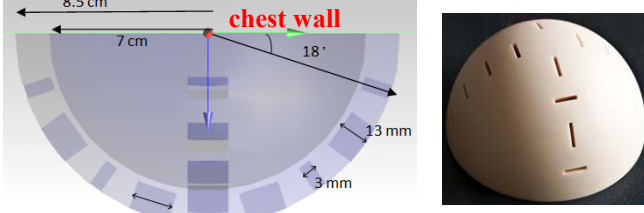


Fig.2 Drawing and photograph of the radome.

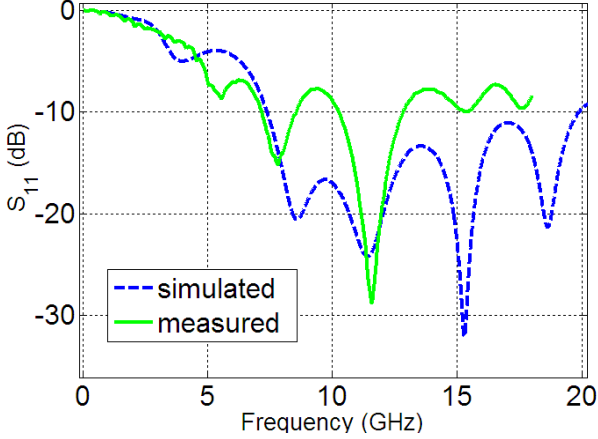


Fig.3 Plot of simulated and measured return loss of the antenna in air.

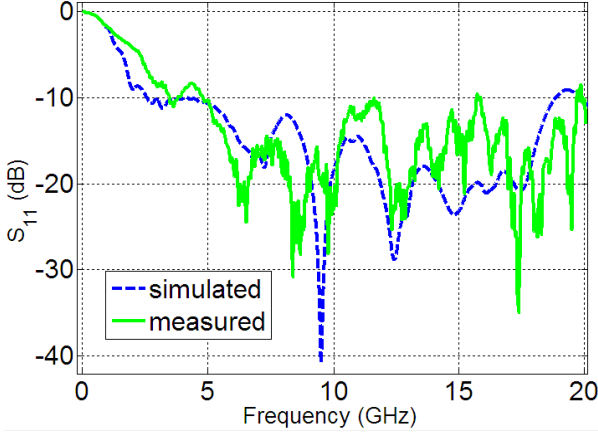


Fig.4 Plot of simulated and measured return loss of the antenna in the radome.

### C. Experimental System

The set-up for our experiment is as follows: a clock (Tektronix, [11], gigaBERT 1400 generator) at 250 MHz drives a picoscope (Pico Technology, [12], PC Oscilloscope 9000) and an impulse generator (Picosecond Pulse Labs, [13], Impulse Generator Model 3600). On every clock signal an impulse of -7.5 V is sent to one antenna, which is held in the radome. A breast phantom is placed inside the radome. In

between the radome and the breast phantom is a roughly 0.5-cm filling of matching medium (the fat-mimicking material). Once the pulse is transmitted from the antenna, it propagates through the radome and the matching medium, into the breast phantom with scattering occurring at all interfaces (for instance, between fat and tumor tissues). The scattered signals are then received by another antenna (the set-up currently only uses two) at a different location in the radome. The received signal is delivered to the picoscope for analog-to-digital conversion and analysis.

### III. RESULTS

These experiments were performed using a phantom with a 2.5-mm skin layer filled with fat. Two sizes of cylindrical tumors were tested – both 3 cm high with diameters of 2 cm and 1 cm. Henceforth, we will refer to these two tumor sizes as large and small, respectively.

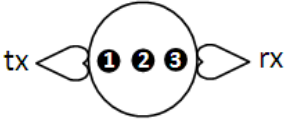
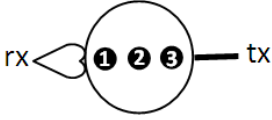
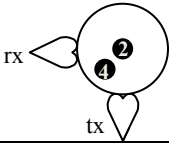
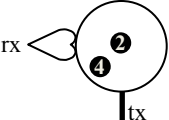
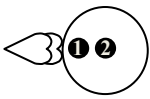
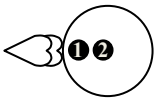
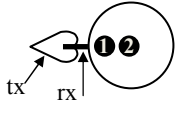
The experiments are performed by first recording a baseline measurement, i.e., when no tumors are present. Then the tumor is placed in the tissue and the new received signal is recorded. The tumor response is calculated as the difference between the received signal with the tumor present and the baseline signal. In this manner, a patient can receive a check-up from a doctor who assures there are no tumors present and then takes ‘healthy-baseline’ measurements with the proposed system. Following the check-up, the patient can at regular intervals have repeat scans with our system. If the system detects a departure of the current measurements from the healthy-baseline then the patient is alerted to undergo further tests.

Several antenna locations were tested to verify the tumor detection abilities of the system; we present seven distinct cases. Table I lists these cases along with a description and diagram of the antenna and tumor positioning for each. The tumor sites are numbered 1 through 4. Site 2 is at the centre of the radome, while sites 1 and 3 are equidistant between the centre of the radome and the radome wall. In cases where the transmitting antenna (tx) and receiving antenna (rx) axes are positioned at 90° within the radome, tumor site 4 is halfway between the centre of the radome and the radome wall, exactly in between the transmitter and the receiver. The diagrams shown for each case are simplified sketches of the top view of the radome measurement set-up (i.e., looking from the chest wall, within the body, into the breast).

For each of the listed subcases, the signal at the receiving antenna is recorded. The maximum received amplitude (denoted as ‘R’), as well as the maximum tumor response (‘T’) calculated for each instance, are also shown in Table I.

The goal in testing these scenarios is two-fold. First, we wish to verify that both the large and small tumor can always be detected regardless of the tumor site and where the antennas are. Second, we aim to determine if there is a certain arrangement of transmit-receive antennas that provide better tumor responses overall. The latter point would allow us to construct a smarter antenna array in the future.

TABLE I  
DESCRIPTION OF PERFORMED MEASUREMENTS, MAXIMUM RECEIVED SIGNAL AMPLITUDES AND MAXIMUM TUMOR RESPONSE AMPLITUDES. THE LARGE TUMOR IS CYLINDRICAL, 3 CM LONG WITH A DIAMETER OF 2 CM. THE SMALL TUMOR IS ALSO CYLINDRICAL WITH A DIAMETER OF 1 CM, HEIGHT OF 3 CM. THE ANTENNAS ARE DEPICTED AS A HEART SHAPE (WHEN PARALLEL TO CHEST WALL) OR A THICK SOLID LINE (WHEN PERPENDICULAR TO CHEST WALL), LOCATED AROUND THE SPHERICAL CROSS-SECTION OF THE RADOME.

Case Description	Subcase	Scenario	R (mV)	T (mV)
<b>Case 1:</b> Co-planar antennas, located 180° apart in the radome. Both in the 2 <sup>nd</sup> slot away from the chest wall. 	1.0	Baseline (no tumor present)	44.60	N/A
	1.1	Large tumor in position 2	46.87	2.27
	1.2	Large tumor in position 1	47.04	4.40
	1.3	Large tumor in position 3	45.37	4.00
	1.4	Small tumor in position 2	45.65	6.65
	1.5	Small tumor in position 1	45.29	4.06
	1.6	Small tumor in position 3	45.73	4.92
<b>Case 2:</b> Antennas oriented at 90° to each other, located 180° apart in the radome. Tx in 2 <sup>nd</sup> slot, rx in 3 <sup>rd</sup> slot from chest wall. 	2.0	Baseline (no tumor present)	6.63	N/A
	2.1	Large tumor in position 2	6.44	1.67
	2.2	Large tumor in position 1	6.54	3.85
	2.3	Large tumor in position 3	5.73	4.67
	2.4	Small tumor in position 2	6.38	2.96
	2.5	Small tumor in position 1	6.77	3.08
	2.6	Small tumor in position 3	5.33	4.77
<b>Case 3:</b> Co-planar antennas, located 90° apart in the radome. Tx in 3 <sup>rd</sup> slot from chest wall, rx in 2 <sup>nd</sup> . 	3.0	Baseline (no tumor present)	60.73	N/A
	3.1	Large tumor in position 2	65.81	6.25
	3.2	Large tumor in position 4	60.96	3.38
	3.3	Small tumor in position 2	64.90	4.71
	3.4	Small tumor in position 4	60.92	1.63
<b>Case 4:</b> Antennas oriented at 90° to each other, located 90° apart in the radome. Both antennas are in the 2 <sup>nd</sup> slot from chest wall. 	4.0	Baseline (no tumor present)	17.73	N/A
	4.1	Large tumor in position 2	21.58	9.88
	4.2	Large tumor in position 4	22.67	11.0
	4.3	Small tumor in position 2	21.15	13.5
	4.4	Small tumor in position 4	22.33	11.0
<b>Case 5:</b> Co-planar antennas, located 0° apart in the radome. Tx in 2 <sup>nd</sup> slot from chest wall, rx in 3 <sup>rd</sup> . 	5.0	Baseline (no tumor present)	120.1	N/A
	5.1	Large tumor in position 2	121.8	12.6
	5.2	Large tumor in position 1	125.0	16.7
	5.3	Small tumor in position 2	118.1	8.00
	5.4	Small tumor in position 1	122.3	12.6
<b>Case 6:</b> Co-planar antennas, located 0° apart in the radome. Rx in 2 <sup>nd</sup> slot from chest wall, tx in 3 <sup>rd</sup> . 	6.0	Baseline (no tumor present)	122.7	N/A
	6.1	Large tumor in position 2	126.7	12.8
	6.2	Large tumor in position 1	120.5	6.06
	6.3	Small tumor in position 2	124.3	3.00
	6.4	Small tumor in position 1	123.7	2.06
<b>Case 7:</b> Antennas oriented at 90° to each other, located 0° apart in the radome. Rx in 2 <sup>nd</sup> slot from chest wall, tx in 3 <sup>rd</sup> . 	7.0	Baseline (no tumor present)	32.77	N/A
	7.1	Large tumor in position 2	33.37	9.67
	7.2	Large tumor in position 1	41.00	23.1
	7.3	Small tumor in position 2	38.92	17.9
	7.4	Small tumor in position 1	36.85	27.2

To show a sample of the time-domain data, we plot one period each of the received signals and the tumor response for two of the seven cases. Figures 5 and 6 plot the received signal amplitude and the tumor response, respectively, for Case 4; Figures 7 and 8 plot the same measured signals for Case 5.

#### IV. DISCUSSION

From Figures 5 and 7, we note that the received signals for each subcase are aligned in time and follow the same trend. Small changes in amplitude due to the presence of a tumor can either increase the maximum received signal or dampen it. For instance, in Table I we see that for Cases 1, 3, 4 and 7, the baseline measurement is less than the received signals with a tumor present. However, in the other cases, the baseline can be greater or less than the received signal depending on the tumor location and size. A tumor can significantly attenuate a signal passing through it, but at the same time the wave scattering off the tumor's surface can be relatively large. The tumors in our set-up were hand-carved and thus do not have smooth surfaces, which contributes to the variability in scattered wave.

For each subcase, the tumor response is clearly detected (see Figures 6 and 8, Table I). Both the large and small tumors can be identified as present regardless of their location or the antenna positions. This indicates that the experimental system is promising and that there is value in recording healthy baseline signals; in practice there are numerous additional challenges that must be addressed.

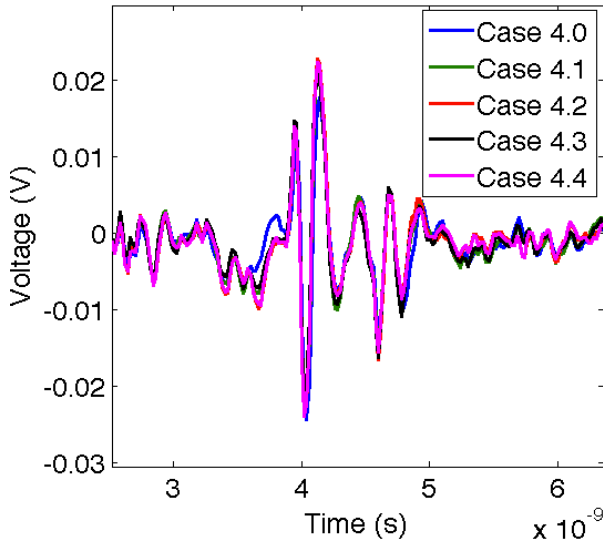


Fig.5 Plot of the received signals for Case 4.

Now, we analyze the results to determine if there is one specific antenna arrangement that is preferential in terms of detection capabilities. From Table I, we see that each scenario with cross-planar antennas gives a smaller received voltage than its co-planar counterparts. As an example, Case 1 tests the reception of signals that have been transmitted through the entire breast phantom with both antennas oriented in the same (horizontal) direction. Case 2 performs the same test as Case 1, except with the antennas oriented at 90° to each other.

The average received signal in Case 1 is 45.8 mV (maximum deviation from the average is 1.22 mV) and only 6.3 mV (maximum deviation of 0.97 mV) in Case 2. Similarly, we note that in Case 3 the received signals are approximately three times larger than those of Case 4; and Cases 5 and 6 give maximum received voltage about 3.5 times greater than in Case 7. From this, we can conclude that reception is always better when the antennas have the same orientation and are parallel to one another.

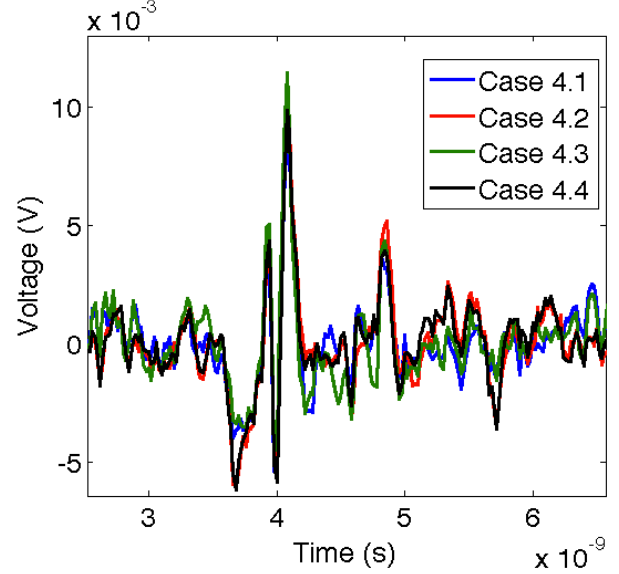


Fig.6 Plot of the tumor responses for Case 4.

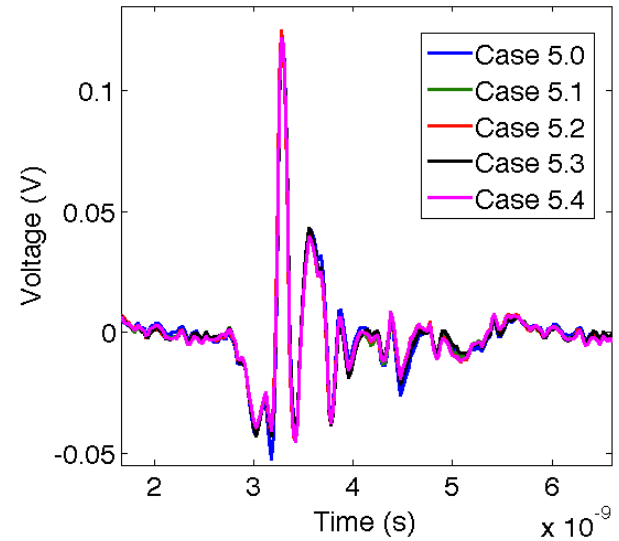


Fig.7 Plot of the received signals for Case 5.

However, a high-amplitude received signal does not necessarily correspond to a larger tumor response than is seen with small-amplitude received signal. This is shown in Table I, exemplified by Cases 3 and 4. In Case 3, the maximum of the tumor response is, at best, only 9.5% of the maximum received signal. Case 4, on the other hand, exhibits tumor responses that are at least 46% of the corresponding received signals. Thus the tumor detection ability in each subcase 4.1 - 4.4 is much improved compared to subcases 3.1 - 3.4.

Finally, we note that the cases that show the best tumor detection are Cases 7 and 5; averaging over the



subcases, the mean maximum tumor amplitudes are 19.47 mV and 12.48 mV, respectively. These two cases are both scenarios in which it is the reflection signal that is measured. Having a system which records the reflected tumor response is beneficial for two reasons: a tumor is always closer to both antennas than the centre point of the phantom, and consequently, the reflected wave travels through less breast tissue and experiences a smaller attenuation.

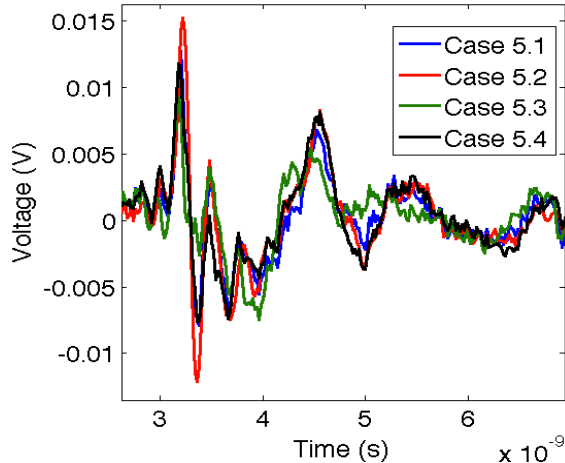


Fig.8 Plot of the tumor responses for Case 5.

It is worthwhile discussing why Case 6 does not exhibit behavior similar to Case 5 when the antenna locations and tumor sites for these cases are the same with the exception that the transmitting and receiving antenna in Case 5 switch roles in Case 6. We can offer the following reasoning. In Case 5, the transmitting antenna is closer to the chest wall and since the tumors are placed in the phantom at the point where the chest wall would be, the wave leaving this (endfire) antenna directly impacts the tumor. In Case 6, the transmitting antenna is located closer to the nipple area and therefore the sent wave power is concentrated further away from the tumor. This effect is exacerbated when a tumor is at site 1, as the transmitted wave nearly bypasses the tumor location altogether. As we note from Cases 5 and 7, a tumor at the closer site 1 leads to a larger tumor response than one at site 2, and this is the behavior we desire from our system.

The analysis of the thorough set of experiments conducted with our proposed breast cancer detection system (39 tests in total) has shown that two antenna arrangements in particular tend to allow for improved tumor detection compared to the other antenna arrangements. These two arrangements are denoted by the diagrams of Case 7 and Case 5 in Table I. In both of these cases the transmit and receive antennas are located as close together as possible and the signal reflected by the tumor (and not transmitted through it) is recorded.

This observation will allow us to design a better antenna array for future measurements. Since it is undesirable to have a single antenna provide both the transmit and receive functions (due to the expense of fast-switching equipment), we will focus on an array that places two antennas as close to co-located as possible. Both antenna configurations from Case 7 and

Case 5 can be incorporated into such an array. The next generation of experiments will also include several more antennas, with groups of ‘co-located’ antennas on each side of the radome. This will give tumors in each quadrant of the breast an equal likelihood of being detected.

## V. CONCLUSIONS

We have presented a time-domain microwave breast cancer detection system. It has been tested with breast phantoms that match actual breast physiology and electrical properties as closely as possible. Tumors of different sizes and locations within the breast phantom were successfully detected. We also experimented with the arrangement of the transmit and receive antennas with respect to each other, and determine two layouts that provide the best tumor detection capabilities.

## ACKNOWLEDGMENTS

The authors would like to acknowledge the support of the Natural Sciences and Engineering Research Council of Canada (NSERC) and Partnerships for Research on Microelectronics, Photonics and Telecommunications (PROMPT).

## REFERENCES

- [1] M. Lazebnik, D. Popovic, L. McCartney, C. Watkins, M. Lindstrom, J. Harter, S. Sewall, T. Ogilvie, A. Magliocco, T. Breslin, W. Temple, D. Mew, J. Booske, M. Okoniewski, and S. Hagness, “A large-scale study of the ultrawideband microwave dielectric properties of normal, benign and malignant breast tissues obtained from cancer surgeries,” *Phys. Med. Biol.*, Vol. 52, pp. 6093-6115, 2007.
- [2] E.C. Fear, P.M. Meaney and M.A. Stuchly, “Microwaves for breast cancer detection?” *IEEE Potentials*, pp. 12-18, February/March 2003.
- [3] I.J. Craddock, A. Preece, J. Leendertz, M. Klemm, R. Nilavalan and R. Benjamin, “Development of a hemi-spherical wideband antenna array for breast cancer imaging,” European Conference on Antennas and Propagation *EUCAP 2006*, Nice, France, 6-10 November 2006.
- [4] M. Lazebnik, E. Madsen, G. Frank and S. Hagness, “Tissue-mimicking phantom materials for narrowband and ultrawideband microwave applications,” *Phys. Med. Biol.*, Vol. 50, pp. 4245-4258, 2005.
- [5] E. Zastrow, S. Davis, M. Lazebnik, F. Kelcz, and S. Hagness, “Development of Anatomically Realistic Numerical Breast Phantoms With Accurate Dielectric Properties for Modeling Microwave Interactions With the Human Breast,” *IEEE Transactions on Biomedical Engineering*, Vol. 55, no.12, pp. 2792-2800, 2008.
- [6] S. Gabriel, R.W. Lau and C. Gabriel, “The dielectric properties of biological tissues: II. Measurements in the frequency range 10 Hz to 20 GHz,” *Phys. Med. Biol.*, Vol. 41, pp. 2251-2269, 1996.
- [7] E. Porter, J. Fakhoury, R. Oprisor, M. Coates and M. Popović, “Improved Tissue Phantoms for Experimental Validation of Microwave Breast Cancer Detection,” European Conference on Antennas and Propagation *EUCAP 2010*, Barcelona, Spain, 12-16 April 2010.
- [8] H. Kanj and M. Popović, “A Novel Ultra-Compact Broadband Antenna for Microwave Breast Tumor Detection,” *Progress in Electromagnetics Research*, vol. 86, pp. 169-198, 2008.
- [9] (2011) Friatec. [Online]. Available: <http://www.friatec.com/>
- [10] (2011) SPEAG, Schmid & Partner Engineering AG. [Online]. Available: <http://www.speag.com/>
- [11] (2011) Tektronix. [Online]. Available: <http://www.tek.com/>
- [12] (2011) Pico Technology Limited. [Online]. Available: <http://www.picotech.com/>
- [13] (2011) Picosecond Pulse Labs. [Online]. Available: <http://www.picosecond.com/>